Journal of Earth Sciences and Geotechnical Engineering, Vol.13, No.2, 2023, 1-22
ISSN: 1792-9040 (print version), 1792-9660 (online)
https://doi.org/10.47260/jesge/1321
Scientific Press International Limited

Evaluation of Geothermal Energy Potential in Parts of the Lower Benue Trough, Nigeria, Using Aeromagnetic Data

Chukwudi C. EZEH[1] and Chukwuebuka J. MAGBO[1]

Abstract

Nine sheets of Regional Aeromagnetic data of parts of Lower Benue Trough were evaluated through the use of Centroid and forward modelling of the spectral peak methods with a view to delineating structures and basin geometry of the Southern (Lower) Benue Trough of Nigeria. Geological cross sections were used to determine the number of anomalies from the residual magnetic map after which the Discrete Fourier Transform method was applied in calculating and computing the depth to the top (Zt), depth to the bottom (Zo), Curie point depth (CPD), geothermal gradient and heat flow. From the results, the depth to the top of the magnetic source ranges between 0.5km and 12.5km with the highest points towards the south - western part of the study area. The depth to the bottom of magnetic source (centroid depth) ranges from 2km to 54km and the highest areas are located towards the north-eastern part of the study area. The geothermal gradient ranged between 21^{o}C/Km to 29.5^{o}C/Km., Ogoja, Oturkpo, and Katsina–Ala are situated within the region of high geothermal gradients (>26.5^{o}C/Km). The heat flow values range from 22mW/M^2 to 74 mW/M^2 and the areas with the high heat flow values are Makurdi, Ogoja, Gboko and Katsina-Ala. The results also show that the Curie temperature isotherm within the study area is not a horizontal level surface, but it is undulating. The study also identified high sedimentary thickness and considerable geothermal potential which could serve as a basis for hydrocarbon accumulation and geothermal exploitation.

Keywords: Geothermal Gradient, heat flow, Crustal Temperature, Geothermal Potentials, Total Magnetic Intensity (TMI).

[1]Department of Geology and Mining, Enugu State University of Science and Technology, Enugu, Nigeria.

Article Info: Received: May 15, 2023. Revised: July 10, 2023.
Published online: July 25, 2023.

1. Introduction

Due to the increasing need for sustainable energy resources, developed and developing countries of the world are looking for alternative energy resources that are clean and renewable. Geothermal energy can be developed as an alternative to fossil fuels, thereby mitigating the negative impact of fossil fuelling on the environment.

Abraham and Nkitnam (2017), observed the presence of thermal and warm springs to be situated in the northern and central portions of the Cretaceous Benue Trough. Geothermal energy is a huge reservoir of thermal energy in the earth interior whose surface manifestation are volcanoes, geysers, ground and hot springs.

Aeromagnetic survey works on the principle that variations in the measured magnetic field of an area reflect the distribution of magnetic minerals in the Earth's crust (Anakwuba et al, 2011). There are varieties of reasons for which the survey is undertaken. They include; geologic mapping, mineral and oil exploration, environmental and groundwater investigations. They are also useful in the detection, location and characterization of magnetic sources. In addition, the use of aeromagnetic data to estimate Curie point depth through which the thermal structure of the earth's crust in various tectonic settings is determined and several authors (Okuba et al., 1985; Blakely, 1988; Okubo and Matsunaga, 1994; Onwuemesi, 1997; Tanaka et al.,1999 and Dolmaz et al., 2005; Chinwuko et al., 2013; Ofor and Udensi, 2014; Nwankwo and Abayomi, 2017) have written extensively on the thermal structure of the crust involving the Curie point depth estimations and geothermal energy potential of some parts of Nigeria.

This research work focuses on the evaluation of high-resolution aeromagnetic data through the use of centroid and forward modelling of the spectral peak method, with a view of delineating structures and basing geometry of the southern (lower) Benue trough, Nigeria. Residual aeromagnetic data was used to determine the depth to the top of the sediment, depth to the bottom (centroid depth), Curie isotherm, geothermal gradient and heat flow. Areas with high heat flow and geothermal gradient have high geothermal reservoirs. This study evaluates the geothermal potential in the study area using heat flow and geothermal gradients by the use of aeromagnetic data.

2. Location and geology of the study area

The geology of the study area is presented in Figure 1. The study area is bounded by latitudes $6^{o}\ 45^{1}$N and $7^{o}\ 30^{1}$N and longitudes $7^{o}\ 30^{1}$ E and $9^{o}\ 30^{1}$E of the lower Benue trough. The total coverage area was about 27,225 square kilometres. The Benue Trough is a major geological formation underlying a large part of Nigeria and extending to about 1000km northeast from Bight of Benin to Lake Chad. The Trough is divided into Lower, Middle and Upper regions. The Anambra Basin in the west of the region is more recent than the rest. The trough was formed by rifting of the central West African basement beginning at the start of the cretaceous. The Lower Benue Trough comprise of the Abakaliki Anticlinorium towards the

Anambra Basin, and Afikpo syncline. The Asu River group found in the Abakaliki-Afipko basins is Albian to Cenomanian, comprising of fluvial regressive arkosic sandstones lying directly on the crystalline basement; this is overlain by the transgressive Eze-aku formation of Turonian age. The Ezeaku formation consists of black shale and siltstones which sits unconformably at the Precambrian Gneiss to the north of Ugep.

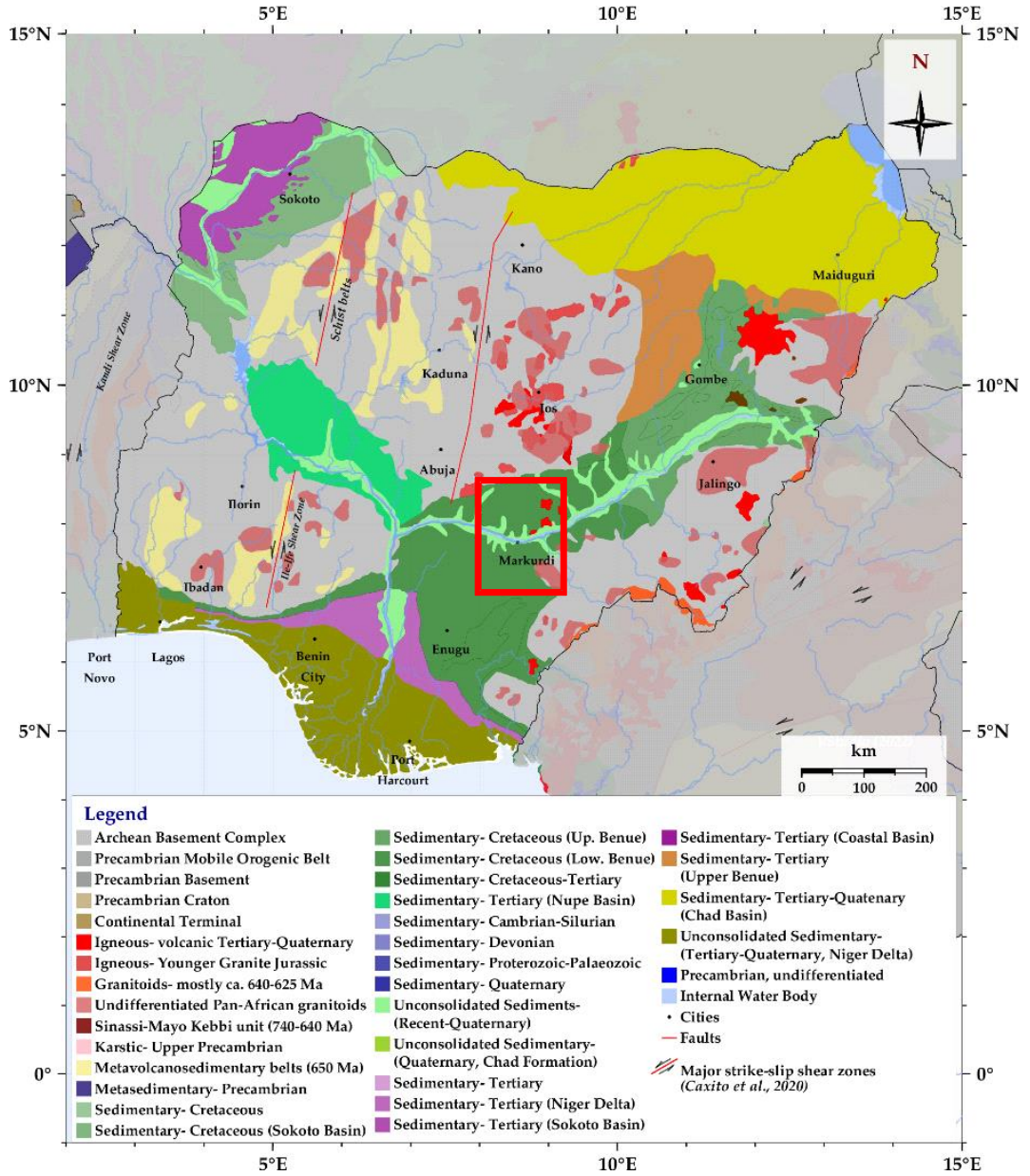

Figure 1: Geological map of Nigeria showing the location of the study area (Modified After Obaje *et al*., 2004).

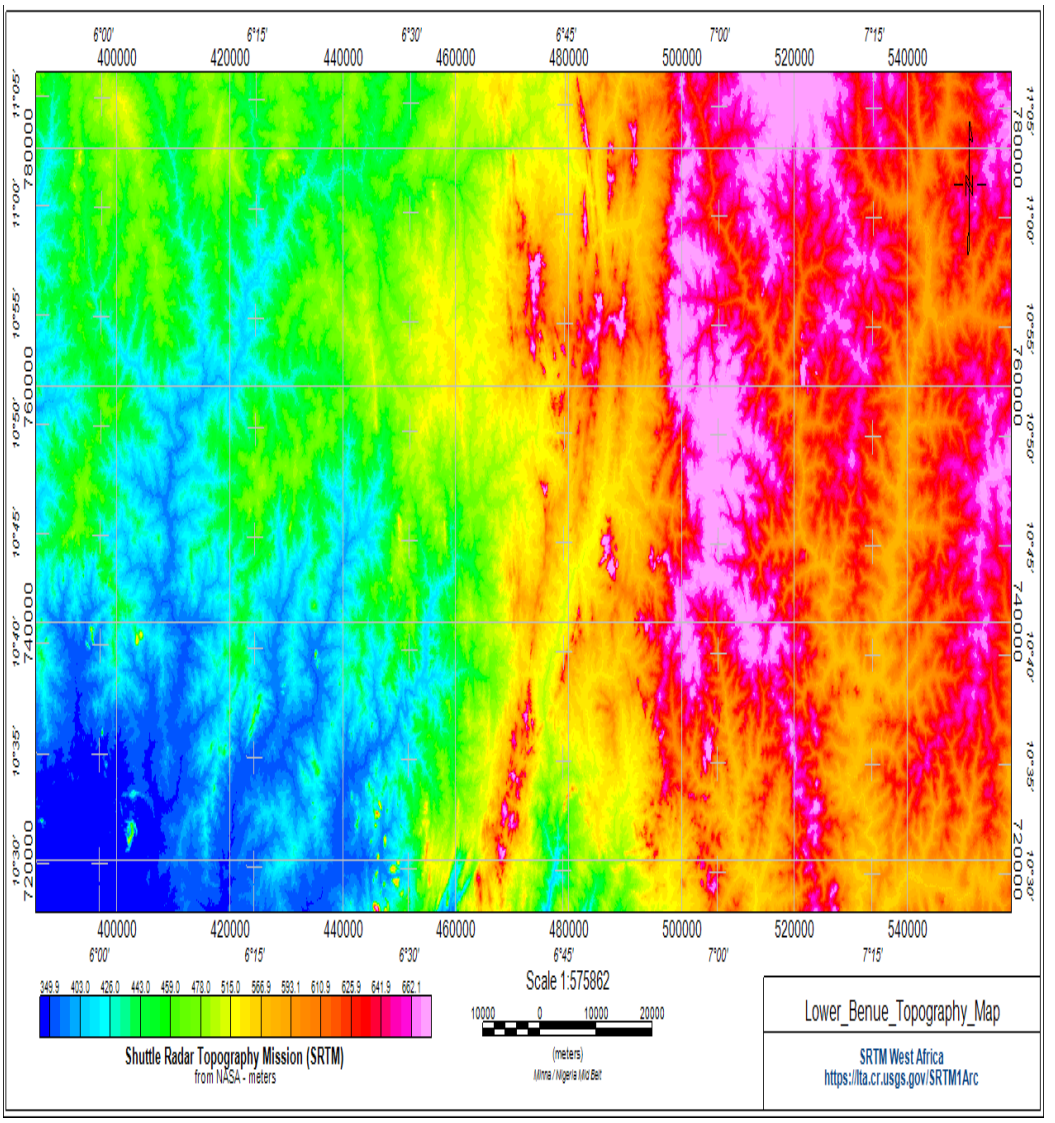

Figure 2: Shuttle Radar Topographic Mission map of the study area.

The SRTM (Short Radar Topographic Mission) map shown above displays the topographic nature of the study area. The elevation ranges from 349.9m to 662.1m. From the map, it is revealed that the eastern (north and south) part of the map has the highest elevation while the north western part of the map reveals moderate elevation and the south western part of the map reveals areas with low elevation.

3. Methodology

3.1 Desktop study, data acquisition and processing

Nine Aeromagnetic Data sheets comprising of sheet numbers 250 (Agana), 251 (Makurdi), 252 (Akwana), 270 (Oturkpo), 271 (Gboko), 272 (Katsina-Ala), 289 (Ejekwe), 290 (Ogoja), 291 (Obudu), were obtained from the Nigerian Geological Survey Agency. The data was acquired and measured by Fugro Airborne Survey (2006)-(2007) on a scale of 1:250,000 series. The survey was carried along Northwest-Southeast lines with a spacing of 500m and flight elevation of 150m above sea level. The magnetic data was obtained from digitization of the total magnetic intensity contour maps on a scale of 1:100,000. The total coverage area was about 27,225 square kilometers. The aeromagnetic data was compared or Geo-referenced to the universal Transverse Mercator coordinate system to ensure effective comparison with other digitized maps of the area.

The procedure involved in this study are digitization of Aeromagnetic map, separation of magnetic data, production of magnetic anomaly and first vertical derivative maps, analysis and modelling of magnetic anomaly data.

The Discrete Fourier Transform is applied to regularly spaced data such as the aeromagnetic data. The Fourier Transform is summarized by (Onwuemesi, 1997).

From spectral analysis results, curie isotherm is calculated using Bhattacharyya and Leu, (1975) method. The first step according to Bhattacharyya and Leu, (1975) is to estimate the depth to centroid (Z_o) of the magnetic source from the slope of the longest wavelength of the spectrum that is given below:

$$In\left[\frac{\rho(\sqrt{S})}{/S/}\right] = InA - 2\pi/S/Z_o \quad (1)$$

where,

P is the radially averaged power spectrum (natural log of amplitude) of the anomaly, /**s**/ is the wave number (Nyguist frequency) and A is a constant.

The second step is the estimation of the depth to the top boundary (Z_t) of that distribution from the slope of the second longest wavelength spectral segment (Okubo *et al*., 1985),

$$In\left[\frac{\rho(\sqrt{S})}{/S/}\right] = InB - 2\pi/S/Z_t \quad (2)$$

where,

B is the sum of constants independent of **/s/.**

Then, the basal depth (Z_b) of the magnetic source was calculated from the equation of Bhattacharyya and Leu, (1975) as shown below:

$$Z_b = 2Z_o - Z_t \quad (3)$$

The obtained basal depth **(Z_b)** of magnetic sources in the study area is assumed to be the Curie point depth according to Bhattacharyya and Leu, (1975).

Hence, the heat flow and thermal gradient value was calculated in the study area using an equation expressed by Fourier's law as follows:

$$q=\lambda \frac{dT}{dZ} \quad (4)$$

where,
q is the heat flow and λ is the coefficient of thermal conductivity.
According to Tanaka *et al*, (1999), the thermal gradient (dT/dZ) can be estimated using equation 4, where we have the Curie temperature (θ) and the Curie point depth (Z_b) available:

$$\theta=\left[\frac{dT}{dZ}\right] Z_b \quad (5)$$

4. Quantitative interpretation of aeromagnetic data

In other to evaluate depths to basement across the study area, five (5) profile lines were taken on the residual map in perpendicular to the direction of the magnetic anomalies, namely A-A^1, B-B^1, C-C^1, D-D^1, E-E^1 (Figure 3). The profile lines in the residual map revealed a total of 24 anomalies. The anomalies were subjected to spectral analysis to estimate the depth to the magnetic source and other parameters like Curie point depth, geothermal gradient and heat flow within the study area.

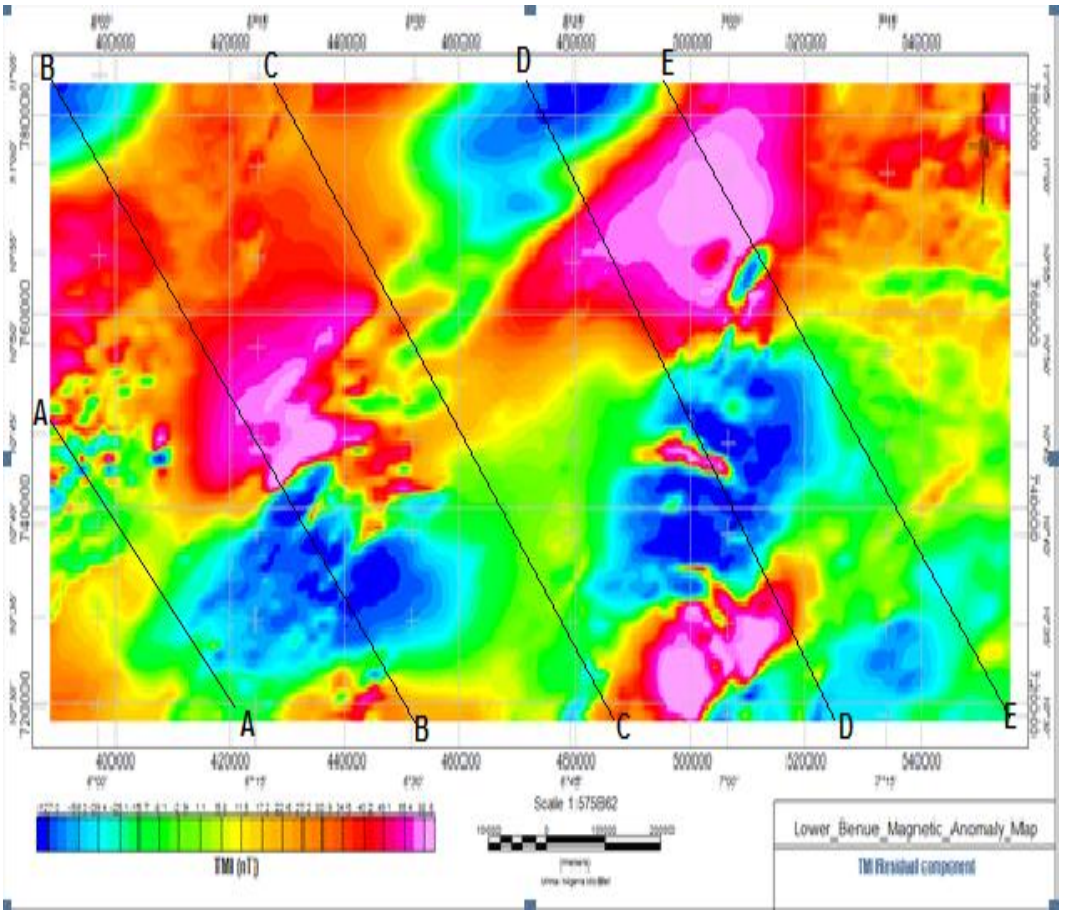

Figure 3: Residual filtered map of the study area with profile lines.

5. Results and Discussion

Table 1: Analysis of the profile lines.

Profile A-A^{l}		Profile BB^{l}		Profile CC^{l}		Profile DD^{l}		Profile EE^{l}	
x(km)	y(km)	x(km)	y(km)	x(km)	y(km)	x(km)	y(km)	x(km)	y(km)
0	40	0	80	0	0	0	100	0	80
0.1	20	0.25	100	0.4	0	0.4	80	0.25	100
0.25	20	0.3	120	0.65	20	1	80	0.5	100
0.7	40	0.35	140	0.85	40	1.1	100	0.65	100
0.85	60	0.5	160	1	60	1.3	100	1.25	100
1	60	0.6	160	1.5	60	1.5	80	1.4	80
1.2	60	0.75	140	1.6	80	1.6	60	1.8	60
1.25	40	1.1	120	2	80	1.9	40	2	60
1.45	20	1.25	140	2.25	60	2.2	20	2.15	40
1.65	20	1.5	140	2.5	60	2.45	20	2.3	40
1.88	20	1.75	120	3.2	80	3	40	2.5	60
2	20	2	100	3.6	80	3.9	20	3.15	60
		2.75	80	3.9	100	4.3	20	4	40
		2.85	60	5	100	4.4	0	4.5	40
		3	40	6.75	100	4.5	-40	4.9	40
		3.6	40	7.4	80	5	-40	5.15	20
		4.75	80	8	80	5.25	0	5.35	0
		5.25	100	8.6	80	5.4	-20	5.6	-20
		5.35	100	9	80	5.5	-40	5.85	-40
		5.75	80	9.5	60	5.75	0	6	-60
		6	60	10	60	6	40	6.2	-60
		6.25	40	10.25	80	6.25	100	6.65	-40
		6.5	20	10.5	80	6.6	100	6.75	-20
		6.75	0	10.75	60	6.75	80	7	0
		7	-20	11	40	7.25	80	7.2	20
		7.1	-40	11.25	40	7.9	80	7.5	40
		7.2	-40	11.5	20	8.2	100	7.9	60
		7.3	-20	12	-20	8.5	100	8.15	80
		7.5	0			9	80	8.9	100
		7.75	20			9.25	60	9.15	100
		7.85	40			10	40	9.35	80
		8.1	60			10.4	40	9.5	60
						11.3	60	10	40
						12.7	60	11	40
						12.8	40	12	60
						12.9	20	12.3	80
						13	0	12.9	80
						13.1	-20	13.1	60
						13.2	-20	13.3	40
						13.7	-20	13.4	20
						13.95	-20	13.7	20
						14.2	0	13.8	40
						14.45	20	13.8	60
						14.7	40	13.9	80
						14.6	40	14	80
						14.95	20		
						15	-20		
						15.15	0		
						15.3	60		
						15.5	80		
						15.75	80		

Table 2: Depth calculation results from spectral analysis.

Anomaly	Depth to the Top (km)	Depth to the Bottom (km)	Curie Point Depth (km)	Geothermal Gradient ^{o}C/km	Heat Flow (mW/m2)
1	12,77460	12,2	11,05	23,4452	61,4509
2	11,67320	13,13	13,7	29,1422	70,3425
3	9,93425	8,76	25,03	22,2346	58,4511
4	9,29714	10,53	22,99	23,2299	60,69958
5	2,61886	5,76	29,04	29,3566	70,23496
6	4,04175	5,14	24,97	24,2452	57,86541
7	4,16683	4,81	23,45	21,1343	59,11938
8	2,78819	5,76	23,17	25,6753	65,56423
9	1,76618	6,09	29,66	29,6544	24,66543
10	1,83936	9,06	30,01	21,4533	23,42341
11	2,89119	3,08	22,26	26,1674	56,45324
12	2,38351	2,79	21,72	24,2456	59,4342
13	0,67320	1,38	30,76	21,4335	30,24532
14	0,71833	9,88	33,34	24,2918	54,25188
15	1,81228	8,78	23,97	29,5693	74,06542
16	1,46625	6,14	20,69	27,1517	70,13242
17	1,19508	7,96	23,93	24,6507	68,4327
18	2,03137	8,12	27,84	28,0235	63,54637
19	2,00309	54,61	23,55	24,248	63,56341
20	1,21583	9,02	24,76	23,5143	64,67549
21	2,10640	8,34	24,25	25,0522	60,6549
22	2,72369	9,07	20,66	28,0875	58,5679
23	2,93912	9,56	23,61	25,8891	69,54657
24	2,64870	4,98	24,61	23,3761	60,56438
Average	3,65452	9,372917	24,12583	25,21964	58,58129583

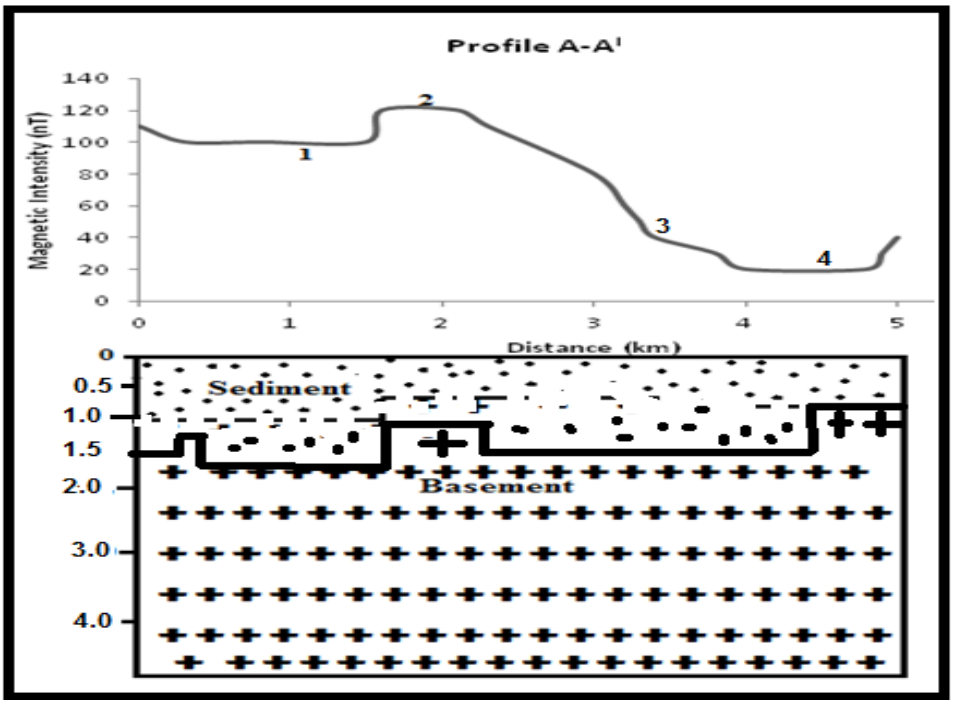

Figure 4: Model profile anomaly along A-A.[I]

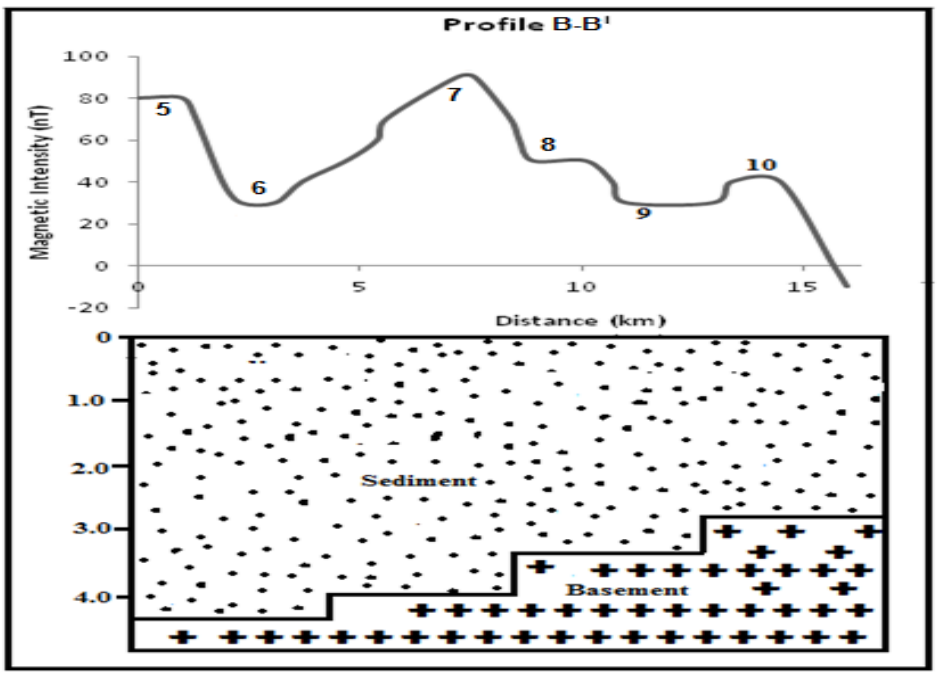

Figure 5: Model profile anomaly along B-B.[I]

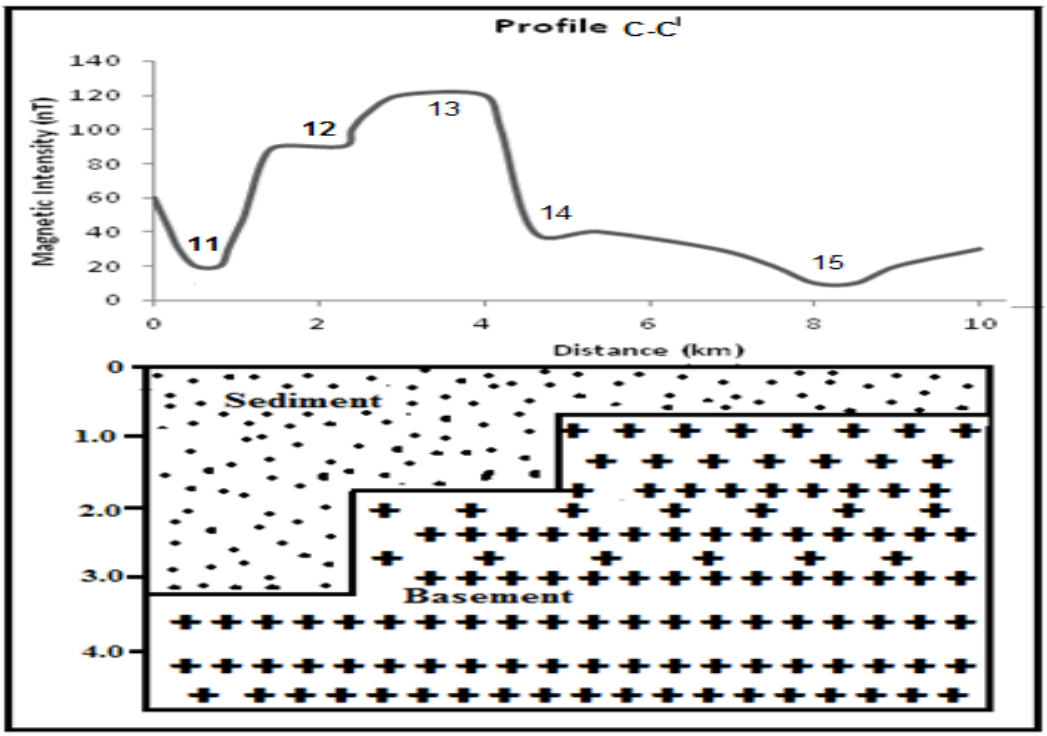

Figure 6: Model Profile anomaly along C-C.^{I}

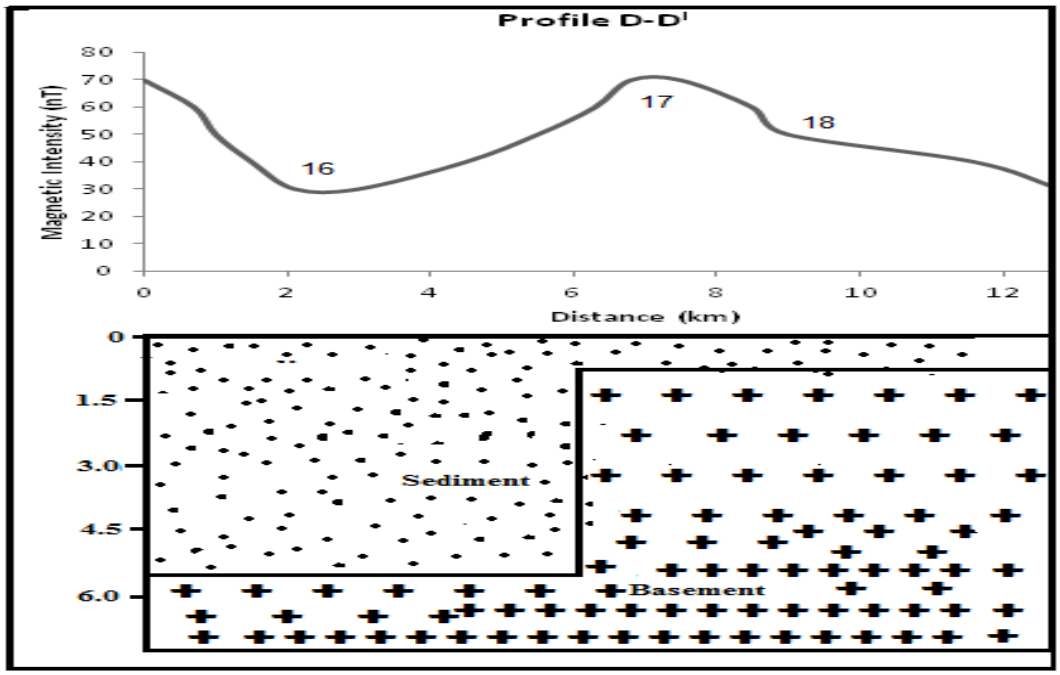

Figure 7: Model Profile anomaly along D-D.^{I}

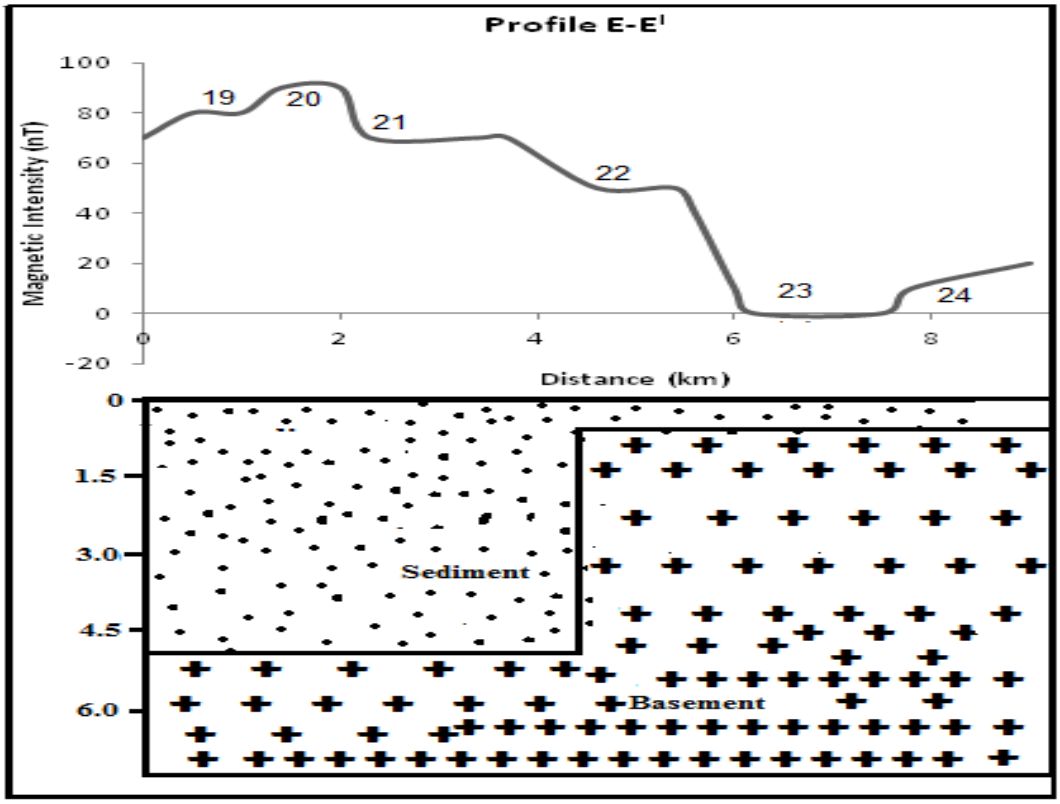

Figure 8: Model Profile anomaly along E-E.^{I}

Figure 9a present the map of the total magnetic intensity (TMI) and Figure 9b the magnetic intensity residual map. The maps indicate that the total magnetic intensity field ranges from 31893 to 32105nT, while the residual map range is from -123.3 to 86.1nT. Both maps show areas with low and high magnetic fields. The two maps revealed that at the North eastern and north western parts of the maps comprising of Akwana, Agana, Oturkpo, there is strong evidence of higher magnetic intensity as well as numerous anomalous bodies within those areas. The contour lines in these areas are closely spaced signifying that the depths to the basement around these areas are relatively shallow according to visual interpretation. The central and south western parts of the study area have contours that are widely spaced signifying that the depth to basement is relatively high in these areas and their magnetic field values are also low. The study area is also faulted and the major fault is trending East-West (E-W) according to Chinwuko et al. 2012.

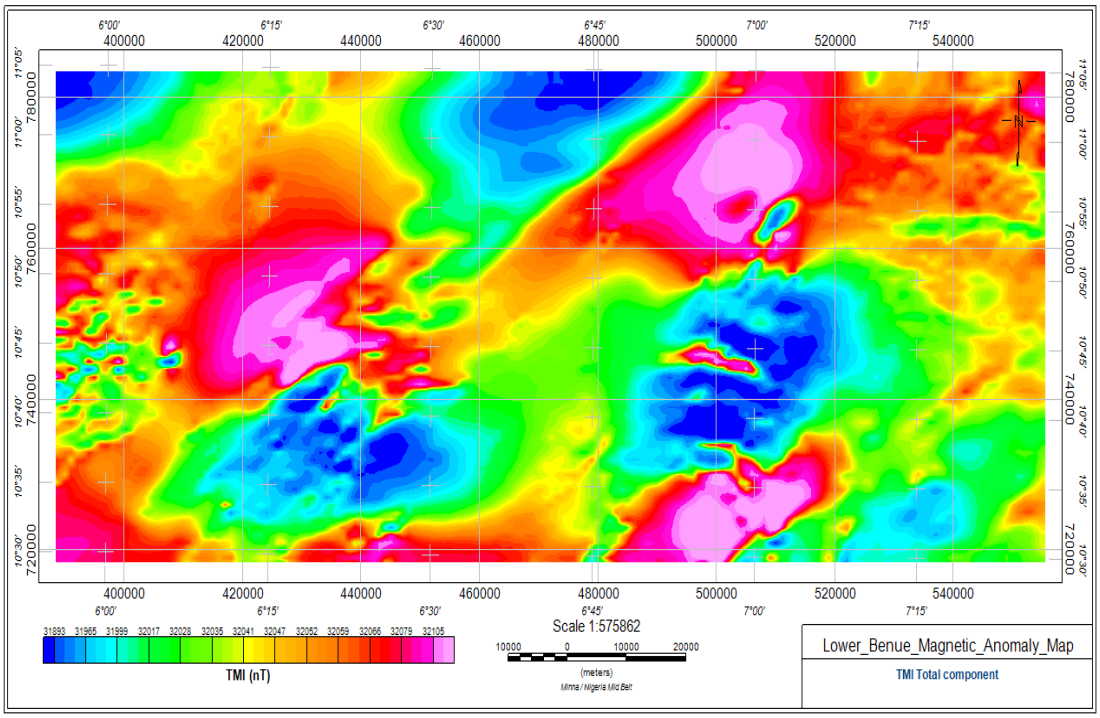

Figure 9a: TMI Magnetic map of the study area.

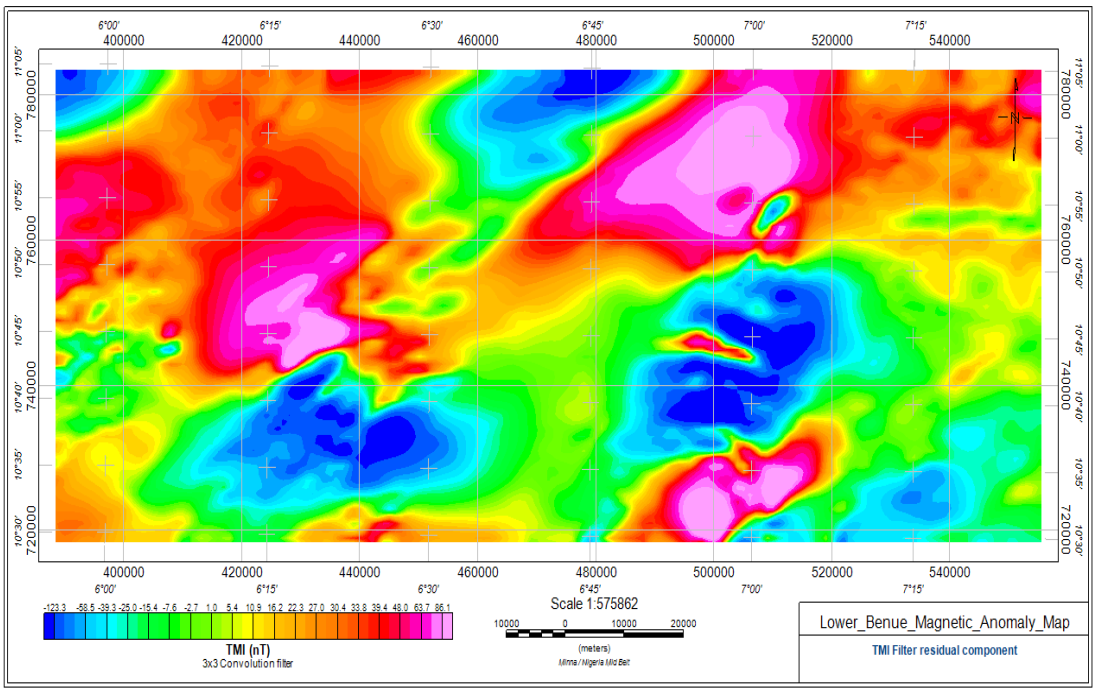

Figure 9b: Residual magnetic intensity filtered map of the study area.

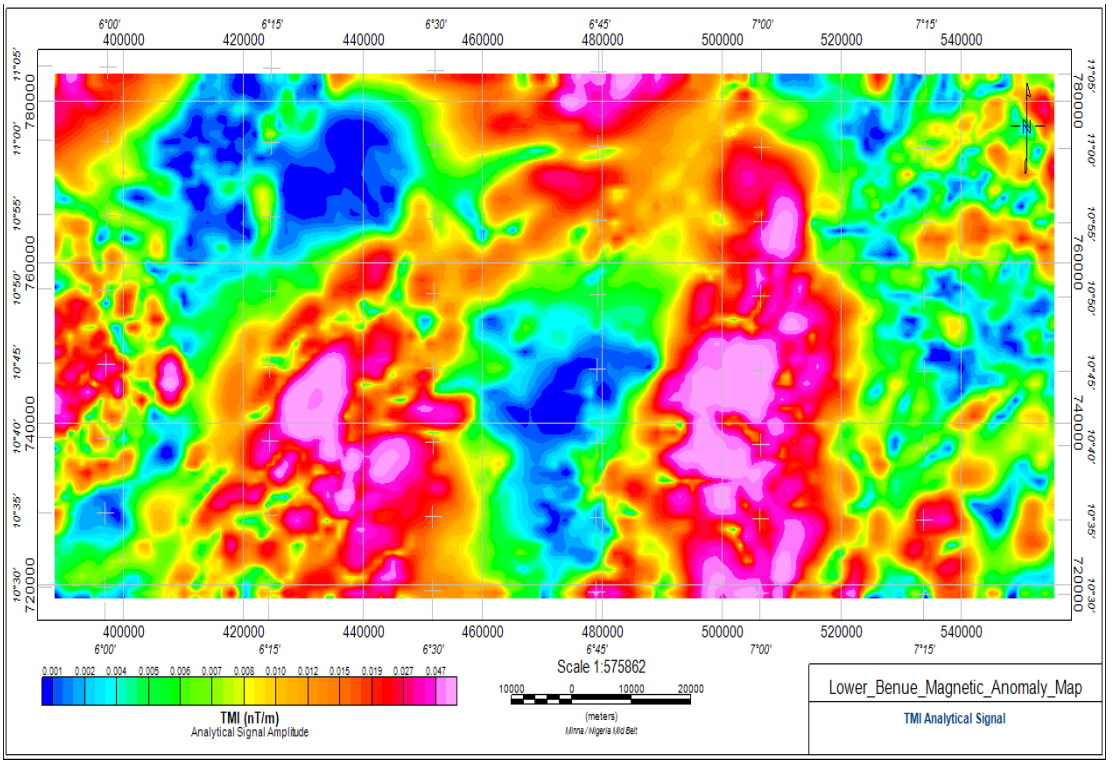

Figure 9c: TMI Analytical Signal Amplitude.

The analytical signal amplitude map (Figure 9c) shows the major anomaly trend within the study area. The trend shows NE-SW and NW-SE directions respectively. The analytical signal amplitude values ranges from 0.001nT/m to 0.047nT/m.

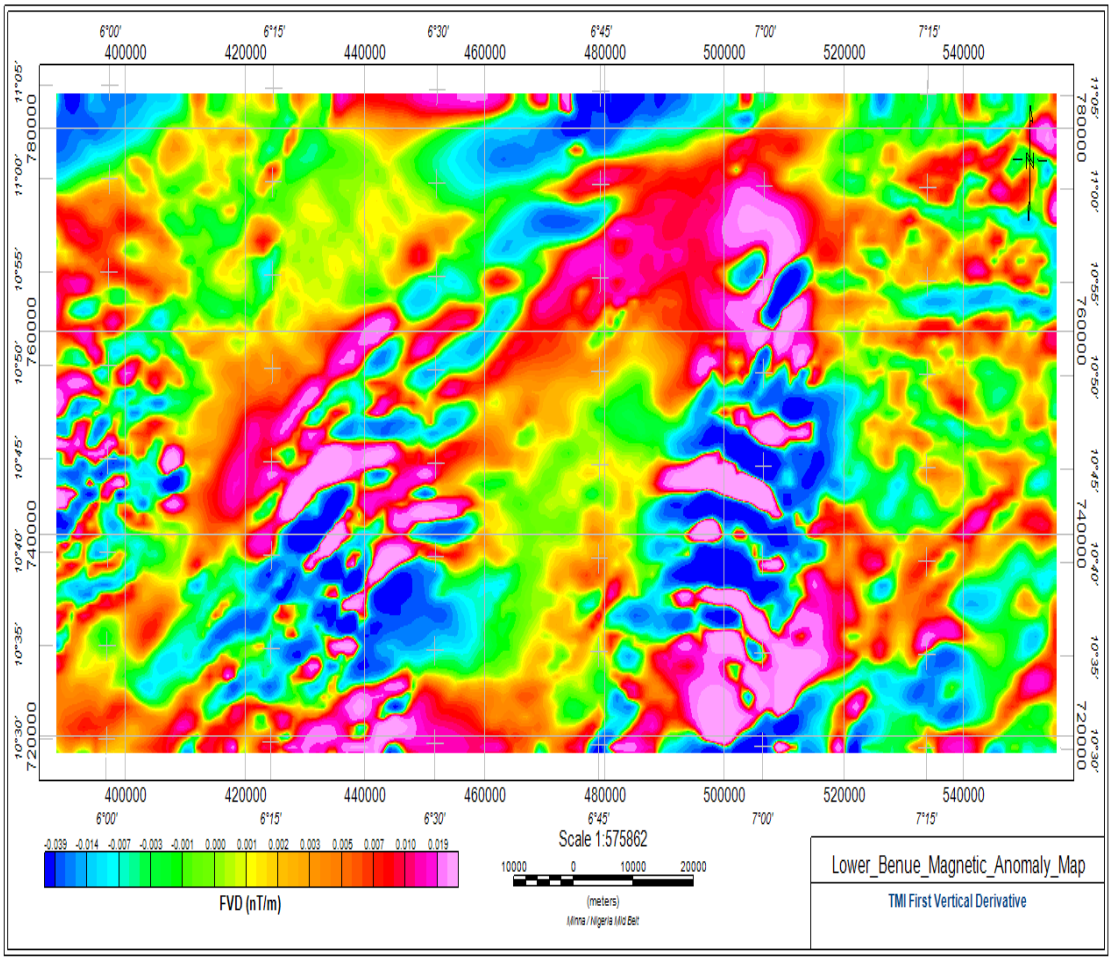

Figure 9d: First vertical derivative map.

The first vertical derivative (FVD) map (Figure 9d) yielded both positive and negative values. The positive values range from 0.001nT to 0.019nT and this could be caused by the presence of the mafic (basaltic) rocks in the study area. While, the negative values range from -0.039nT to -0.001nT and this also could be attributed to the presence of felspathic rocks with high concentration of feldspar, silica and minerals like quartz, muscovite and so on. From the FVD map, the south eastern, south western and north eastern parts of the map show massive occurrences of mafic and felspathic rocks, while at the north central parts of the map, is sparsely scattered.

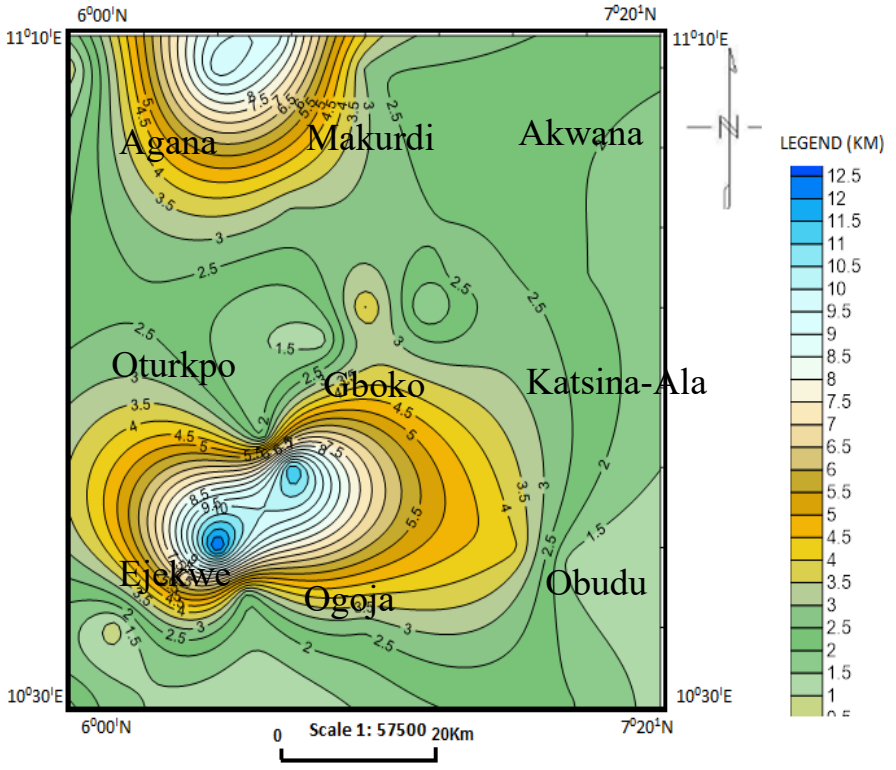

Figure 10: Map of depth to the top of the anomalous body of the study area (Contour interval~ 1km).

From the spectral depth map of the depth to the top of the anomaly (Figure 10), it can be observed that the deepest depth is within the south western and north western parts of the map (2D map) ranging from values of about 12km. The area comprises of Ejekwe, Ogoja, Agana and Markudi area. While the north eastern part and south eastern part of the map reveals areas with shallow depth to the top of the anomalous body.

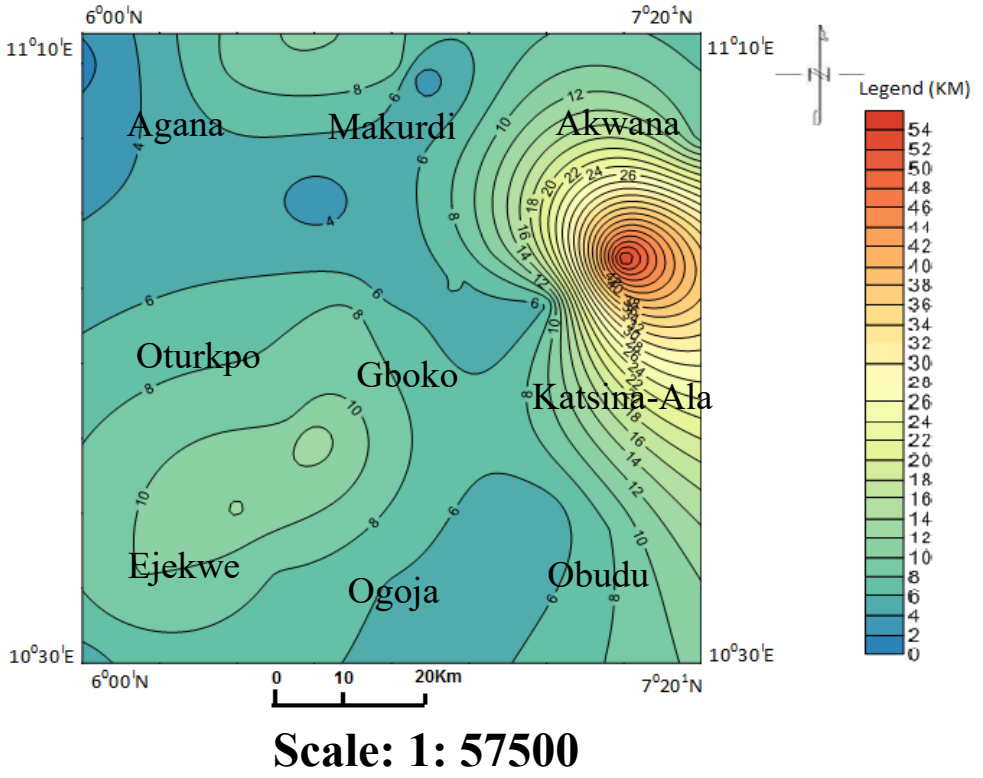

Figure 11: Map of depth to the bottom of the anomalous body of the study area (Contour interval~ 1km).

The map of the depth to the bottom of the anomalous body (Figure 11) reveals that the area with the highest depth to the bottom of the anomalous body is within the north eastern part of the map comprising of Katsina-Ala and part of Akwana areas. The depth value ranges from about 20km to 50km, while the remaining portion of the map has moderate to shallow depth to the bottom of the anomalous body.

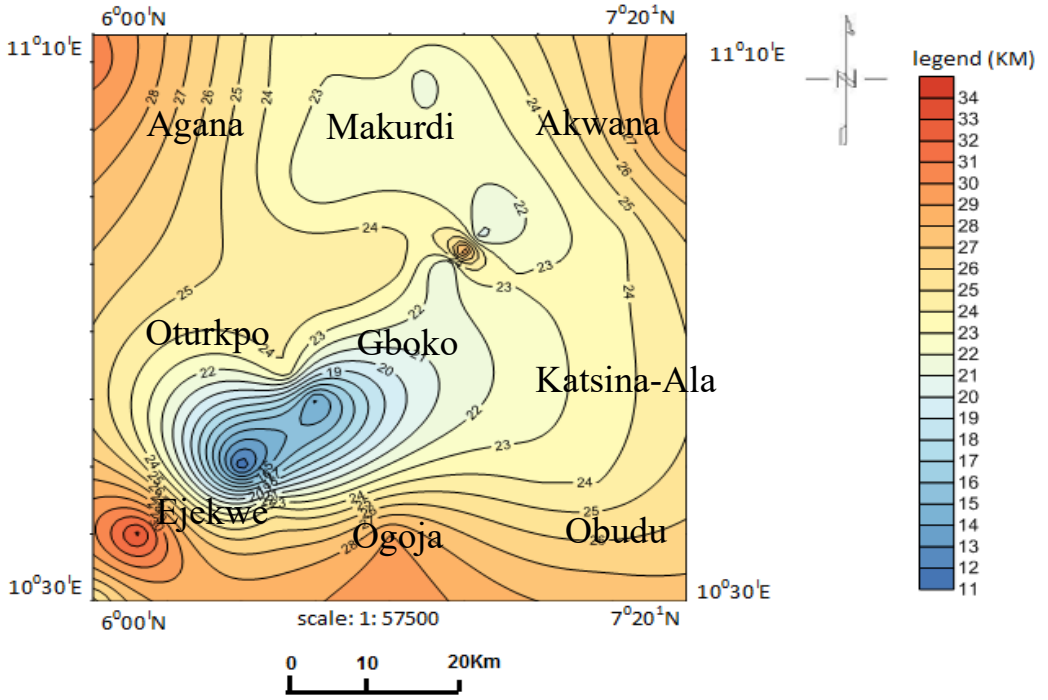

Figure 12: Curie isotherm depth map of the study area

The Curie point depth (Figure 12) of an area is generally dependent on the geological regime of the area, presence of geological structures like faults and synclines. It is also dependent on geological processes like tectonic activities, volcanic eruptions and presence of basement complexes. From the Curie isotherm depth map (Figure 12), it can be observed that the trend of the increment is in NE-SW direction. And the area with the shallowest depth is within the south western part of the map with a value range between 11 and 19km. While the entire north eastern and north western part including the south eastern parts of the map has high Curie isotherm depth values ranging from about 20km to 32km. According to Tanaka et al 1999, Curie point depth shallower than 10km is for volcanic and geothermal fields, from 15km to 25km predicts island arcs and ridges, deeper than 20km predicts plateaus and trenches. Tanaka suggests that the areas comprising of high heat flows and high Curie depth values correspond to areas of volcanic, basement complex, metamorphic regions etc.

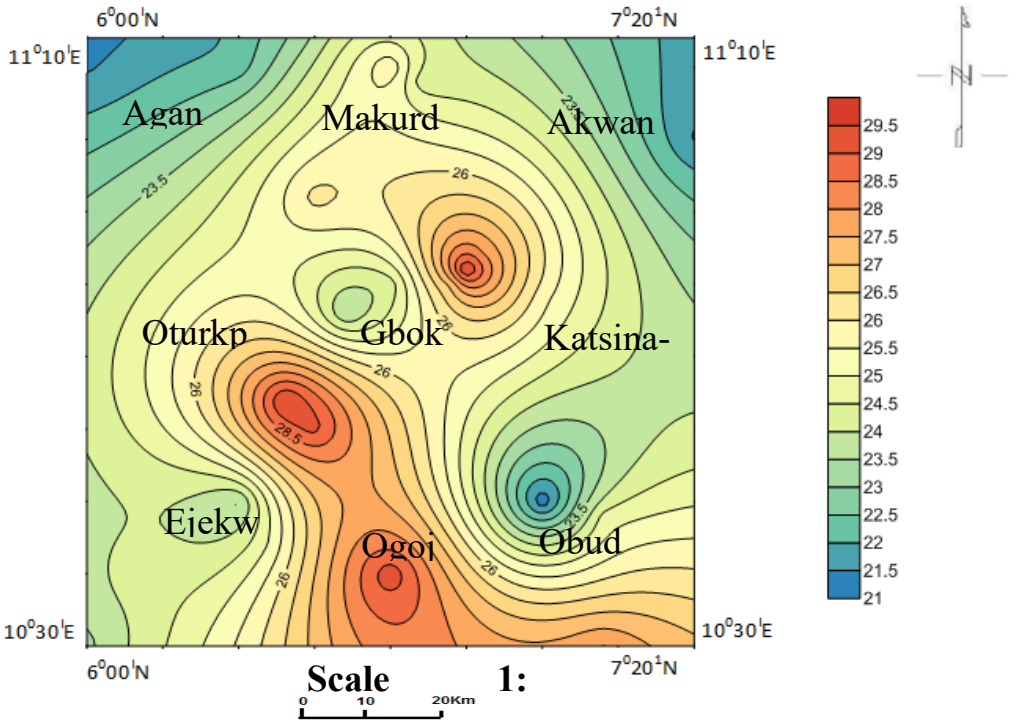

Figure 13: Geothermal gradient map of the study area.

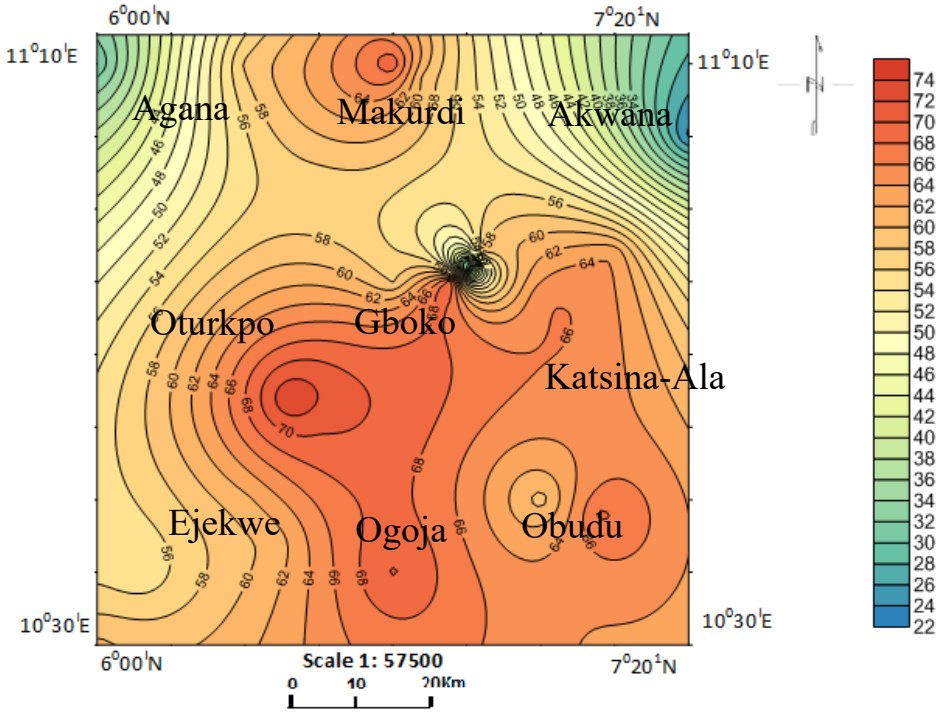

Figure 14: Heat flow map of the study area.

Correlation between geothermal gradient and heat flow shows a positive relationship which means that areas with high geothermal values will likely have high heat flow values. From both map (Figure 13 and Figure 14), it is revealed that south eastern portion of the study area and north central areas has both high geothermal gradient and heat flow values. The geothermal gradient ranges from about 25^0C/km to about 28.5^0C/km within the area and the heat flow value ranges between 54mW/m^2 and 70mW/m^2 in this area two. Then, the eastern and north western part of the maps reveals areas of both moderate to low geothermal gradient and heat flow values. The low to moderate geothermal gradient values ranges from 21^0C/km to 24^0C/km while the low to moderate heat flow value ranges from 22mW/m^2 to 48 mW/m^2 respectively.

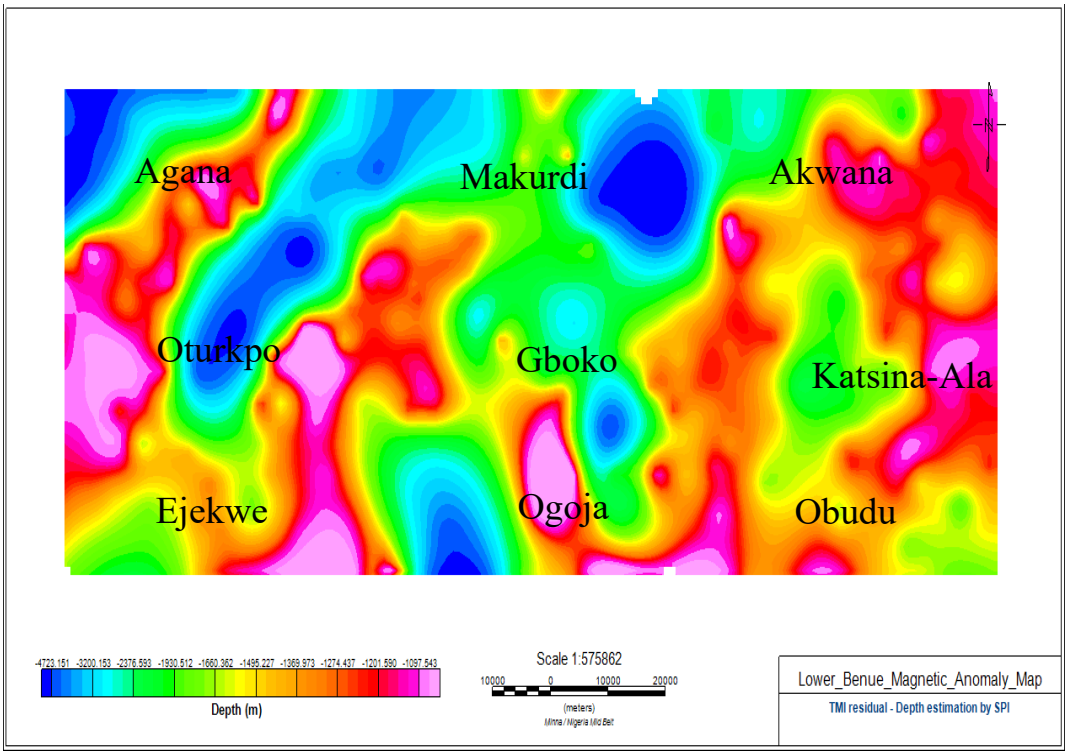

Figure 15: Total Magnetic Intensity (TMI) depth estimation map of the study area from spectral analysis.

6. Summary and Conclusion

Generally, basement depth within the study area was estimated along 5 profile lines using Discrete Fourier Transform of aeromagnetic data. The TMI depth estimation map (Figure 15) reveals that the depth to the basement generally has ranges in depth and include the area with low depth, moderate depth and high depth (thicknesses). The area with low depth includes the Oturkpo area and part of Makurdi axis. While the areas with moderate depths (thickness) are around Gboko and Katsina-Ala areas. The area with high depth (thickness) is seen around Ogoja, Agana, Obudu and Ejekwe areas. However, based on the computed sedimentary thickness (Figures 10 and Figure 11), the geothermal gradient (21-29.5 ^{o}C/Km.) (Figure 13), and heat flow (22mW/M^2 - 74 mW/M^2) (Figure 14), there is possibility of geothermal energy generation within the areas of high TMI depth values (Figure15) and they are around the south eastern–north eastern part of the map and some portion of the south western part of the map (Figure 15).

The high sedimentary thickness and presence of prevalence fractures within the study area, may serve as a migratory pathway for hydrocarbon and geothermal fluid that generates geothermal energy. These pathways could make feasible the possibility of hydrocarbon generation in the study area (Emujakporue and Ekine, 2014). The areas with low sedimentary thickness (low geothermal potential) could possibly house the mineral ore deposits located within the study area.

REFERENCES

[1] Abraham, E.M. and Nkitnam, E.E. (2017). Review of Geothermal energy reserve in Nigeria; the Geo Science fonts. International Journal of Earth Science and Geophysics, 13, p.15.

[2] Blakely, R.J. (1988). Curie Temperature isotherm analysis and tectonic implications of Aeromagnetic data from Nevada. Journal of Geophysical research (93), pp.11817-11832

[3] Bhattacharryya, B.K., and Leu, L.K. (1975). Spectral analysis of gravity and magnetic anomalies due two-dimensional structures. Geophysics, 40: pp.993-1031.

[4] Chinwuko, A. I., Onwuemesi, A. G., Anakwuba, E. K., Okeke, H. C., Onuba L.N., Okonkwo, C.C. Ikumbur, E. B. (2013). Spectral Analysis and Magnetic Modeling over Biu – Damboa, Northeastern Nigeria. IOSR Journal of Applied Geology and Geophysics, 1(1): pp.20- 28.

[5] Chinwuko, A.I., Onwuemesi, A.G., Anakwuba, E.K., Onuba, L.N., and Nwokeabia, N.C. (2012). The Interpretation of Aeromagnetic Anomalies over parts of Upper Benue Trough and Southern Chad Basin, Nigeria. Advances in Applied Science Research,3(3): pp.1757-1766.

[6] Emujakporue, G. O and Ekine, A. S. (2014). Determination of Geothermal Gradient in the Eastern Niger Delta Sedimentary Basin from Bottom Hole Temperatures, Journal of Earth Sciences and Geotechnical Engineering, 3: pp.109-114.

[7] Nwankwor, L., Abayomi, J.S. (2017). Regional estimation of Curie point depth and succeeding geothermal parameters from recently acquired high resolution Aeromagnetic data of the entire Bida Basin, north-central Nigeria. Geothermal energy science 5(1): pp.1-9.

[8] Dolmaz, M.N., Hisarli, Z.M., Ustaomer, T and Orbay, N. (2005). Curie point depths based on spectrum analysis of Aeromagnetic data west Anatolian extentional province, Turkey. Pure and Applied Geophysics 162(3): pp.571-590.

[9] Obaje, N.G.J, Wehner, H., Hamza, H., Scheeder, G. (2004). New geochemical data from the Nigerian sector of the Chad Basin: Implications on hydrocarbon prospectively. Journal of African Earth Sciences, 38(5): pp.477-487.

[10] Okubo, Y.J., Graf, R., Hansen, R.O., Ogawa, K., Tsu, H. (1985). Curie point depth of the Island of Kyushu and surrounding areas. Japan Geophysics, (53): pp.481-491.

[11] Okubo, Y.J., Matsunanaga, T. (1994). Curie point depth in northeast Japan and its correlation with regional thermal structures and seismicity. Journal of Geophysical research (99): pp.22363-22371.

[12] Onwuemesi, A. G. (1997). One dimensional spectral analysis of aeromagnetic anomalies and curie depth isotherm in the Anambra Basin of Nigeria. Journal of Geodynamics, 23(2): pp.95-107.

[13] Ofor, P., Udensi, E. (2014). Determination of the heat flow in the Sokoto basin Nigeria, using spectral analysis of Aeromagnetic data, Journal of Natural sciences research (4): pp. 83-93.

[14] Tanaka, A.Y., Okubo, Y. and Matsubayashi, O. (1999). Curie point depth based on spectrum analysis of the magnetic anomaly data in East and Southeast Asia, Tectonophysics, 396: pp.461-470.